International Journal of Power Electronics and Drive Systems (IJPEDS)
Vol. 14, No. 1, March 2023, pp. 444~452
ISSN: 2088-8694, DOI: 10.11591/ijpeds.v14.i1.pp444-452

Performance analysis of voltage sensorless based controller for two-stage grid-connected solar PV system

Meghraj Morey[1], Nitin Gupta[1], Man Mohan Garg[1], Ajay kumar[2]
[1]Electrical Engineering Department, Malaviya National Institute of Technology, Jaipur, India
[2]Department of Electrical and Electronic Engineering, Birla Institute of Technology, Mesra, India

Article Info

Article history:

Received May 22, 2022
Revised Oct 3, 2022
Accepted Oct 24, 2022

Keywords:

DC-link voltage control
Grid-connected
Power quality
Power-sharing
Sensorless
Solar photovoltaic
Two-stage converter

ABSTRACT

In this research, a sensor free DC-link voltage controller based multifunctional inverter is proposed for a two-stage three-phase grid-connected solar photovoltaic (PV) system. First, the proposed scheme consists of an outer voltage controller requiring DC-link voltage knowledge, has the ability to manage power-sharing between the PV system and the utility grid, and second, has the ability of the VSI to act as a compensator for harmonics in the grid current polluted by non-linear loads. The suggested active power controlling grid reference current signal scheme replaces the standard controller, requiring the high voltage sensor to sense DC-link voltage, which is pricey, increasing the hardware complexity and reducing reliability. The performance of the proposed active power management approach is comparable to that of a conventional voltage sensor-based voltage controller. The effectiveness of the proposed method for two stage three-phase grid-connected solar PV system under fixed and variable irradiance feeding nonlinear loads is rigorously verified using MATLAB/Simulink software.

Corresponding Author:

Meghraj Morey
Electrical Engineering Department, Malaviya National Institute of Technology
Jaipur-302017, India
Email: 2021ree9065@mnit.ac.in

1. INTRODUCTION

Nowadays, the demand for electrical power across the globe is increasing at an alarming rate. The availability of non-renewable sources of energy is depleting rapidly has increased the electric utilities' concern regarding the need to develop alternative, renewable, and sustainable sources of energy [1], [2]. Among the RES, solar photovoltaic (PV) energy is a sustainable and clean way to produce electricity for humankind, which has attracted the attention and investment in the world recently and is one of the key elements in the proliferation of distributed energy generation (DEG) systems [3]. Furthermore, usage of a variety of nonlinear loads has increased by manifolds in the commercial and industrial sectors nowadays, has worsened the problem of non-sinusoidal currents into the electrical power network, which is adversely affecting the reliable operation and efficiency of the power system [4]–[9]. Therefore, improving the power quality (PQ) in the electrical distribution system has become an area of interest among researchers.This need has given rise to enhance PV generation system functionality. In addition to supplying appropriate active power into the grid or meet load demand, the system should also provide power quality conditioning [10].

Attempts have been made in the past to solve utility PQ issues such as current harmonics, decline in point of interfacing (PoI) voltage, load unbalancing, and low power factor in electric distribution systems [11], [12]. To handle the PQ problems in distribution networks, the synchronous reference frame theory (SRF) [13], IcosΦ [14], instantaneous symmetrical component theory [15], and instantaneous reactive power theory (IRPT) [16] based control algorithms have been discussed in depth.

The study presented in Zakzouk *et al*. [17] proposes a decentralized control mechanism for the effective management of power flow from PV systems to the grid through a hybrid DC-DC converter for a three-phase system. A multifunctional inverter along with feeding power to grid from a solar PV system, based on direct power control methodology is addressed in [18] without using sensors for the converter. Bengourina *et al.* [19] presented a Kalman observer, to estimate the PV parameters like voltage and current, thus reducing the number of physical sensors and giving input to the MPPT algorithm [20], [21] to have the maximum power from PV. It is worth mentioning that in [22], a fixed value of grid voltage is used to generate the reference active current, which is not adaptable for any variation in voltage at POI. Based on the paper [23], [24], decoupling capacitor DC voltage is estimated based on solar PV parameters and fixed grid voltage, whereas DC voltage estimation proposed in this paper using solar PV parameters and peak amplitude of the voltage at the point of interface between grid and load.

To address the aforementioned PQ issues, VSI functioning as a harmonic compensator was introduced due to connected non-linear load. An active power current reference generation technique based on a synchronous reference frame (SRF) is employed in this system, pperforms power management in conjunction with grid as per the availability of power from solar PV. A DC-link voltage controller with the proposed DC voltage estimator eliminating the need of voltage sensor on DC side is suggested.The hardware complexity, such as sensor circuitry, signal conditioning circuit, cost, and size, is further reduced as a result. MATLAB/Simulink software was used to make the suggested controller, which was used to test the VSI's multi functionality under various operating conditions for active power sharing and harmonic current compensation.

2. SYSTEM DESCRIPTION

The proposed two-stage grid-interfaced solar PV system is shown in Figure 1, and it is used to generate a power of 3.7 kW for simulation studies. It consists of a solar PV array, first-stage DC-DC boost converter, a decoupling capacitor, and a second-stage VSI connected to three-phase AC utility feeding a linear and/or nonlinear load. A decoupling capacitor connects the output of the boosted DC voltage to VSI. An interfacing inductor is used between PoI and VSI output terminals for smoothening the VSI current before feeding the load and/or grid. VSI currents are controlled and used to get the right amount of active power sharing and to get rid of the effects of harmonics in grid current.

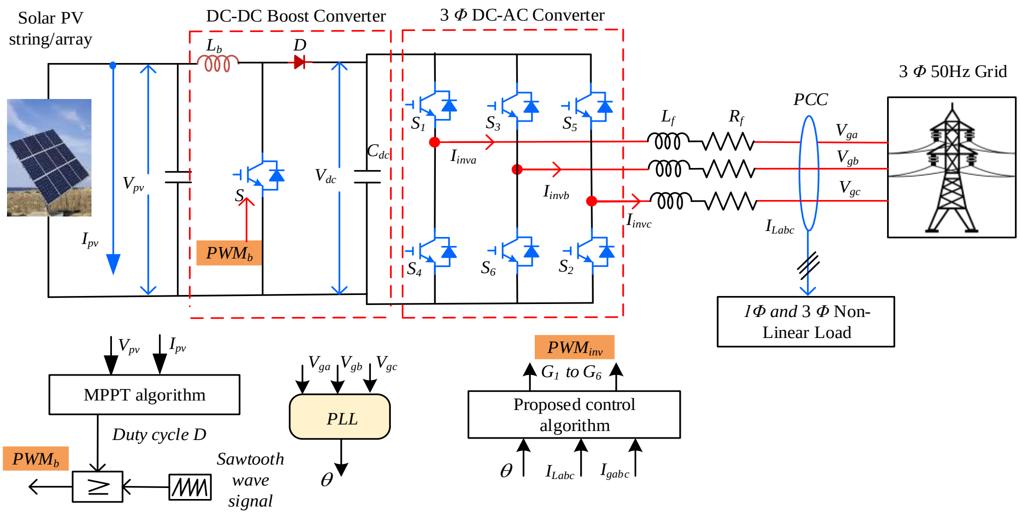

Figure 1. Structure of two-stage three-phase grid integrated solar PV system

2.1. Selection of PV array

To design a 3.7 kW system, the selected solar PV panel has a voltage (V_{mpp}) of 29.3 V and current (I_{mpp}) of 7.47 A at the maximum power point. For the proposed system, 17 panels are connected in series to form a solar PV array generating power of 3.7 kW. The perturb & observe (P&O) based maximum power point tracking (MPPT) algorithm [20], [21] was used to track the PV array's maximum power point. In order to reach the MPP, the reference voltage changes the duty cycle in response to the change in power. It also looks at how the PV array is pointed toward the MPPT. Solar PV array output power can be calculated by, $P_{mp} = N_s \times V_{mp} \times N_p \times I_{mp}$, $P_{mp} = 17 \times 29.3 \times 1 \times 7.47 = 3720W$. where, the number of panels connected in series is N_s while the number of panels connected in parallel is N_p

2.2. DC-DC boost converter

A DC-DC boost converter consist of an inductor, a power switching device (MOSFET or IGBT) and a diode as shown in Figure 1. The pulse for the PWM_b is generated such that maximum power is harnessed from the solar PV panel and minimum voltage V_{dc} is produced at the input of VSI. Selected solar PV panel has a voltage of 29.3 V at maximum power and 17 such panels connected in series producing a voltage of 498 at the input port od DC-DC converter. A duty ratio of 0.32 is considered [25] to produce a output voltage of V_{dc} =730 V, $V_{dc} = \frac{V_{in}}{1-D}$, where V_{in} is DC-DC converter input voltage is equal to PV array output voltage.

2.3. Selection of optimal DC-link voltage magnitude

The magnitude of DC-link voltage at the input of VSI should be more than twice the peak of the per-phase voltage of the three-phase system and is calculated using the following mathematical relation [6].

$$V_{dc} = \frac{2\sqrt{2}V_{LL}}{\sqrt{3}m} \quad (1)$$

Where, modulation index, m is chosen as '1' and V_{LL} is the grid line voltage, selected as 415 V.

The minimum DC-link voltage magnitude can be computed as by (2).

$$V \frac{P_{pv}}{SF^{*}I_{rated}}{}_{dcmin} \quad (2)$$

Where, SF is the safety factor and I_{rated} is current for which system is designed. The DC-link reference voltage should be higher than the line voltage peak. The voltage of the adaptive DC-link is calculated as [19].

$$V_{dc} = \alpha\sqrt{3}V_t \quad (3)$$

Where, α is safety factor accounting the VSI switching losses, interfacing inductor resistance.

For safety side, α is considered as 1.25. v_t is maximum amplitude of voltage at PoI which is calculated as (4).

$$v_t = \sqrt{\frac{2}{3}(v_{sa}^2 + v_{sb}^2 + v_{sc}^2)} \quad (4)$$

Where, v_{sa}, v_{sb}, and v_{sc} are grid phase voltages. To keep the safety margin, a DC-link voltage of 730 V is selected in the proposed system.

3. METHOD

3.1. Model of grid-side converter system

The grid-side VSI employs PWM and vector control approaches to generate the reference signal for the controller. If V_{dinv} and V_{qinv} are the components of the d-axis and q-axis of VSI output voltage in the *d-q* reference frame, and V_{dc} is DC-bus voltage. If the amplitude of a triangular wave in a PWM signal generator is 1V, the *d* and *q* axis voltage vectors required to generate gate signal are given by (7).

$$V_{d\_nom} = V_{dinv}\frac{2}{V_{dc}} \text{ and } V_{q\_nom} = V_{qinv}\frac{2}{V_{dc}} \quad (5)$$

Therefore, the amplitude modulation ration of PWM generator is $m_a = \sqrt{(V_{d\_nom}{}^2 + V_{q\_nom}{}^2)}$ and the peak phase voltage of VSI output can be extracted.

$$V_{inv} = \frac{m_a \times V_{dc}}{2} \quad (6)$$

An interface inductor connects the solar PV system to the electric grid. The relationship between the grid voltage and the converter output voltage in terms of current and grid filter parameters in the *abc* and *dq* axis reference frames has been defined in (9) and (10), respectively, using Kirchhoff's voltage law. The (9) indicates the voltage balancing across the grid filter.

$$\begin{bmatrix} v_{ainv} \\ v_{binv} \\ v_{cinv} \end{bmatrix} = R_f \begin{bmatrix} i_a \\ i_b \\ i_c \end{bmatrix} + L_f \frac{d}{dt} \begin{bmatrix} i_a \\ i_b \\ i_c \end{bmatrix} + \begin{bmatrix} v_{ag} \\ v_{bg} \\ v_{cg} \end{bmatrix} \quad (7)$$

Transforming above equation in *dq* reference frame using Clark’s and Park’s transformation as (8).

$$\begin{bmatrix} v_{dinv} \\ v_{qinv} \end{bmatrix} = R_f \begin{bmatrix} i_d \\ i_q \end{bmatrix} + L_f \frac{d}{dt} \begin{bmatrix} i_d \\ i_q \end{bmatrix} + \omega_g L_f \begin{bmatrix} -i_q \\ i_d \end{bmatrix} + \begin{bmatrix} v_{dg} \\ v_{qg} \end{bmatrix} \quad (8)$$

Where ω_g is the angular frequency of the grid voltage. with space vectors theory, above equation (10) can be written as (11),

$$\bar{v}_{dqinv} = R_f \bar{\imath}_{dq} + L_f \frac{d\bar{\imath}_{dq}}{dt} + j\omega_g L_f \bar{\imath}_{dq} + \bar{v}_{dqg} \quad (9)$$

where, $\bar{v}_{dqinv}$, $\bar{\imath}_{dq}$ and $\bar{v}_{dqg}$ are the instantaneous converter voltage, line current and grid voltage space vectors respectively. Under the steady state, in the above equation derivative term becomes zero, hence can be re-written as,

$$\bar{v}_{dqinv} = R_f \bar{\imath}_{dq} + j\omega_g L_f \bar{\imath}_{dq} + \bar{v}_{dqg} \quad (10)$$

The *q*-component of the grid voltage is rendered zero by using the grid voltage phase angle as the reference phase angle for the *dq* transformation. As a result, the grid side converter *dq*- output voltage can be represented in the form of currents and grid voltage by using (13).

$$\begin{aligned} v_{dinv} &= R_f i_d + L_f \frac{di_d}{dt} - \omega_g L_f i_q + v_{dg} \\ v_{qinv} &= R_f i_q + L_f \frac{di_q}{dt} + \omega_g L_f i_d \end{aligned} \quad (13)$$

Where,v_{dg} represents the amplitude of the grid voltage. The above set of equations governs how the GISPV system is currently controlled (15). Second, as illustrated in Figure 2, the filter inductor current is fed back by the PI compensator. The utility is expected to be stiff. The output current reference generated controls commands for the active current that manages active power and, if desired, allows the reactive power coefficient to be set to zero. If reactive power control is desired in this system, a reactive power reference must be imposed on the system if the reactive power must be regulated. a *d*-axis current reference responsible for the amount of real active power supplied to the load and injected to the grid as per the availability of solar PV power generated. The desirable control objectives are as following:

– Set the V_{dc} DC-link voltage to a specific value.
– To design a reliable system to facilitate active power sharing between solar PV systems and the grid,
– based on power availability and irradiance uncertainty.
– Ensure that the grid current is sinusoidal and free of harmonics at all times.

3.2. DC-link voltage controllers

The theoretical evolution given in [6] and [26] is taken into consideration in the transfer function of the DC-link voltage control loop. As a result, the DC-link voltage's open-loop transfer function can be presented as (14).

$$G_{dc}(s) = \frac{\hat{V}_{dc}}{\hat{\imath}_d} = \frac{3v_d}{2sCV_{dc}} \quad (14)$$

Where, v_d −represents the grid voltage amplitude in rotating reference d-frame, V_{dc} − is the DC-link voltage, and C − is the DC-link capacitance. Thus, the DC-link voltage controller for the three-phase system is represented by the block diagram as shown in Figure 3. Considering the DC-link voltage PI controller (PI), the open-loop and the closed-loop transfer functions can be represented, respectively, by (22) and (23).

$$G_{dcOL}(s) = \frac{3(K_{pdc} v_d s + K_{idc} v_d)}{2s^2 CV_{dc}} \quad (15)$$

$$G_{dccL}(s) = \frac{\hat{V}_{dc}(s)}{\hat{V}^*_{dc}(s)} = \frac{3K_{pdc}v_d s + 3K_{idc}v_d}{2s^2CV_{dc} + 3K_{pdc}v_d s + 3K_{idc}v_d} \quad (16)$$

Where, K_{pdc} and K_{idc} are DC-link voltage controller gain values.

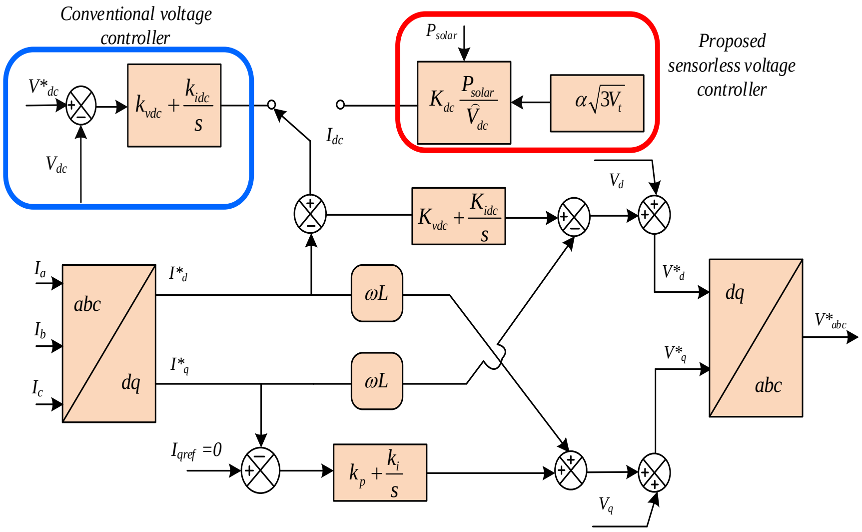

Figure 2. Conventional and proposed DC-link voltage controller

3.3. Active power controlling current signal generation

As illustrated in [19], the reference DC-link voltage is calculated in (3). The DC-link voltage changes as the irradiance level changes. There is always need a sensor to acquire the knowledge of DC-link voltage input of the inverter. To track reference DC-link voltage value, the suggested approach does not require a physical voltage sensor to acquire the knowledge of the DC-link voltage. The net amplitude of the current is estimated as,

$$I_{dcloss} = \frac{P_{solar}}{\hat{V}_{dc}} \quad (17)$$

where, P_{solar} is the extracted maximum power from solar PV array calculated by measuring PV voltage and current. $\hat{V}_{dc}$ is estimated using (3) and (4). Estimated value of DC link voltage depends upon the maximum amplitude of voltage at POI. This current I_{dcloss} is operated upon by a gain to adjust its value such that net current required to compensate for loss within VSI switches, grid interfacing inductor and, is fed to the current controller as shown in Figure 3.

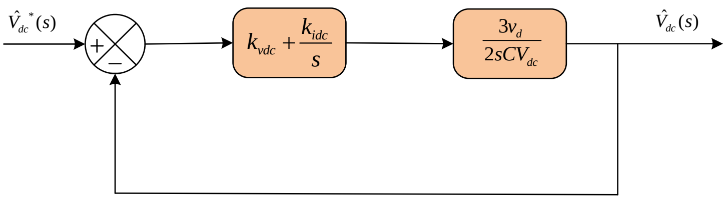

Figure 3. Basic structure of a DC-link voltage controller

4. RESULTS AND DISCUSSION

Table 1 shows the parameters employed in the proposed system employing two-stage grid-connected PV system. The controller's efficacy for a system utilizing a standard DC-link voltage controller is assessed using a rigorous MATLAB/Simulink simulation result. The performance of the DC-link voltage controller without a DC voltage sensor is also tested using the suggested approach. To validate the system performance, system is operated in the following modes,

- System performance during fixed irradiance feeding nonlinear load.
- System performance during gradual and rapid varying irradiance.
- System performance with the proposed DC-link controller without voltage sensor.

4.1. Case I: Performance of the system under static condition

The suggested SRF-based control strategy to provide the active power demand of nonlinear loads under fixed irradiance conditions efficiently controls the functioning of PV supplied VSI, as shown in Figure 4. In the case under consideration for this study, load requires an active power of 8 kW in any given operational situation. While doing so, the nonlinear load generates an active power demand which is totally met by the utility grid only during the time interval t = 0.15 to 0.5 seconds. The PV system, on the other hand, begins injecting active electricity into the utility grid at t = 0.5 seconds. As a result, the entire load power demand is managed based on the DC-link terminal's active power availability (8-3.7= 4.3 kW) and the utility grid's active power availability. Figures 4(a) and 4(b) depicts inverter current waveform when only grid is feeding the load and load demand meet by grid and solar PV system, respectively. Load power demand shown in Figure 4(c) is 8 kW and Figure 4(d) the load power sharing in after 0.5 seconds is 3.7 kW supplied by PV and 4.3 kW by grid. In addition to achieving unity poor factor operation, a DC-link terminal voltage is kept close to the desired reference value, as shown in Figure 4(e).

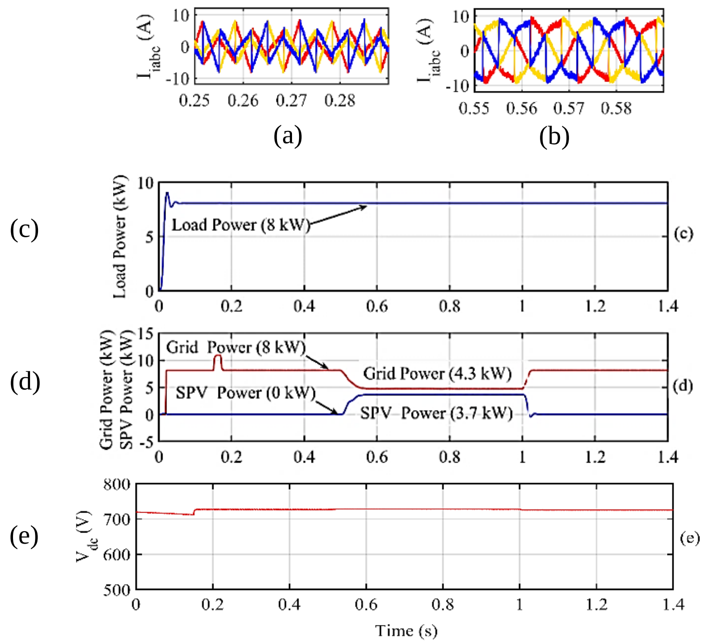

Figure 4. System Performance under static condition current: (a) inverter compensating current when PV is not connected, (b) inverter compensating current when PV is connected, (c) load power, (d) grid power and PV power waveform, and (e) DC-link voltage

4.2. Case II: Performance of the system under variable irradiance condition

As demonstrated in Figure 5, the grid-tied PV system's functionality is confirmed for gradual and step changes in solar irradiation. The solar power generation increases with increasing irradiance (variation ramps from 600 W/m^2 to 1000 W/m^2) during the period from t = 0 to 2 sec, and the grid current waveform is maintained sinusoidal, ensuring active PV power sharing to the load as well as compensation for distorted grid current is shown in zoomed figures for grid voltage, grid current, and inverter current presented in Figures 5(a), 5(b), and 5(c). Furthermore, as shown in Figures 5 (d), and 5(e), the compensating inverter current waveform. The load power supply, solar PV power generation and grid power sharing is achieved as shown in Figures 5 (f) and 5(g). During the time interval t = 2.5 to 3.5 sec, the irradiance is reduced from 1000 W/m^2 to 700 W/m^2, the PV power is reduced to 2.2 kW, and the remaining load demand of 5.8 kW is met by the utility grid illustrated in Figure 5(f). Figure 5(h) shows how well the DC-link voltage controller works and keeps its value close to the 730 V reference value. As a result, it has been proven that the proposed system works better even under dynamic settings.

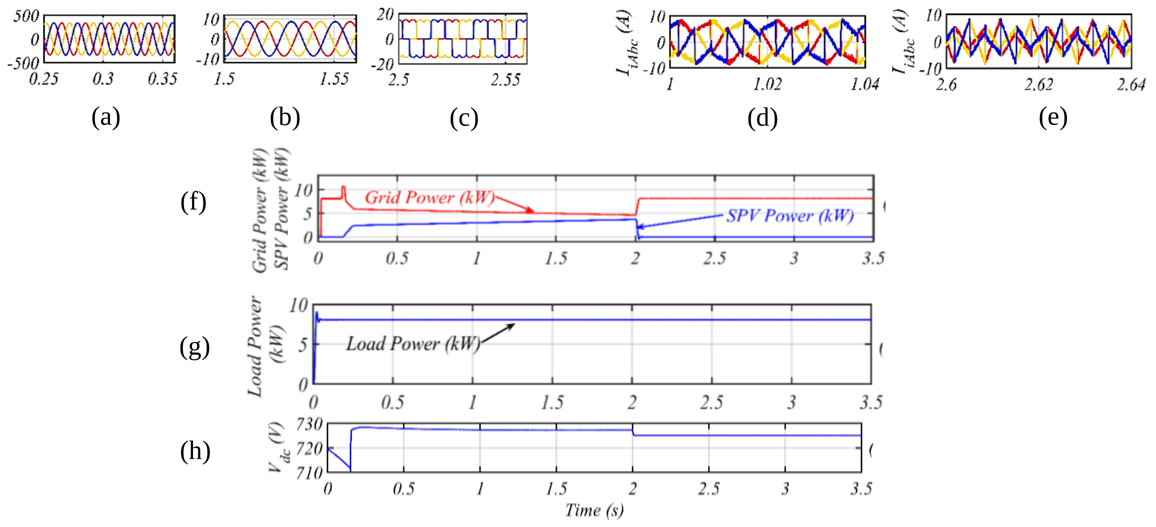

Figure 5. System Performance under dynamic condition: (a) grid side voltage, (b) grid side current, (c) load side current, (d) inverter compensating current when irradiance is gradually changed, (e) inverter compensating current when irradiance is suddenly changed, (f) power sharing between grid and solar PV system, (g) connected load, and (h) DC link voltage

4.3. Case III: System performance without a DC link voltage sensor

The performance of the system with proposed DC-link voltage estimator is verified for fixed irradiance at 1000 W/m^2 represented in Figure 6. Figures 6(a), 6(b) and 6(c) depicts the grid voltage, grid current and load current waveforms, respectively. The grid's current waveform profile becomes sinusoidal along with active power sharing is achieved. Figure 6(d) shows the grid power and PV power generated and it's sharing as per demand. Figure 6(e) presents the estimated DC voltage value very close to the reference value. This confirms the effectiveness of the proposed control algorithm without sensing the DC- link voltage sensor in active power sharing and enhances the grid current profile.

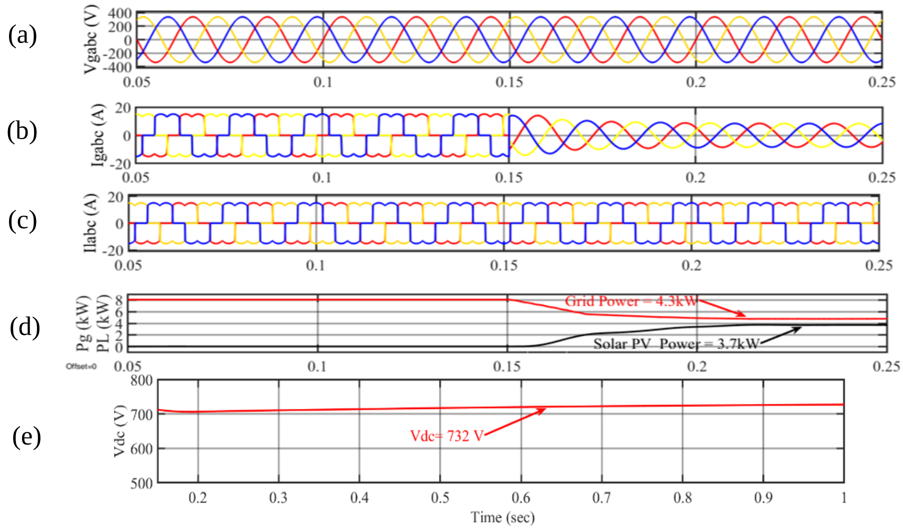

Figure 6. System performance without a DC link voltage sensor: (a) grid voltage, (b) grid current, (c) load current, (d) grid power and PV power waveform, and (e) estimated DC-link voltage

Table 2 shows the comparison of the performance of the MFGC PV system with sensor-based DC voltage and proposed DC voltage estimator without sensor. DC link voltage is maintained at the desired value. Hence with the proposed DC voltage estimator the need for costly voltage sensor can be eliminated. Specifications of the parameters of grid connected system used in simulation are illustrated in Table 1.

Table 1. System specifications

Parameters	Values	Parameters	Values
Boost inductor, Capacitor switching frequency	$L_b = 4.5mH, C_b = 1000\mu F$, $f_{sw} = 20kHz$	PV array output maximum voltage	V_{mpp}= 498.1V
Interfacing inductor	L_f= 8.5 mH,	Nonlinear load parameters and Total Load P_L	R_L= 40 Ω, L_L= 120 mH, I_L= 14A, P_L= 8 kW

Table 2. Details of power sharing and comparison of DC link voltage with and without sensor

P_L(kW)	P_{pv} (kW)	P_g (kW)	V_{dc} (V) using sensor	V_{dc} (V) using Proposed estimator
8	0	8	729.65	731.73
8	3.7	4.3	728.35	732.35

5. CONCLUSION

In this paper, SRF based a control algorithm for a two-stage grid-interfaced PV system with the multi-function capability of VSI for supplying nonlinear load under various uncertain environment is presented. A DC-link voltage controller with the estimated DC link voltage is proposed, giving the satisfactory performance as that of using a physical sensor. This reduces cost, hardware complexity and overall size of the system significantly. When solar power is not available, VSI compensates harmonics current injected by nonlinear load. The proposed controller ensures that the system supports the load demand power as per availability from PV system under fixed and varying solar irradiance, reducing the burden on utility grid. Also, enhancing the grid current profile under various operating conditions supplying the nonlinear load found effectively.

REFERENCES

[1] Q. Jing, Z. Xu, Y. Zheng, D. Wang, and Z. Y. Dong, "Distributed generation and energy storage system planning for a distribution system operator," *IET Renew. Power Gener.*, vol. 12, no. 12, pp. 1345–1353, 2018, doi: 10.1049/iet-rpg.2018.5115.

[2] A. Sangwongwanich, Y. Yang and F. Blaabjerg, "A sensorless power reserve control strategy for two-stage grid-connected PV systems," *IEEE Trans. on Power Elect.*, vol. 32, no. 11, pp. 8559–8569, Nov. 2017, doi: 10.1109/TPEL.2017.2648890.

[3] A. Kumar, N. Gupta, and V. Gupta, "A Comprehensive review on grid-tied solar photovoltaic system," *Journal of Green Engineering, River Publications*, vol. 7, no. 1, pp. 213 – 254, 2017, doi: 10.13052/jge1904-4720.71210.

[4] M. Bouderbala, B. Bossoufi, A. Lagrioui, M. Taoussi, H. A. Aroussi, and Y. Ihedrane, "Direct and indirect vector control of a doubly fed induction generator based in a wind energy conversion system," *Int. J. of Elect. and Comp. Engg. (IJECE),* vol. 9, no. 3, pp. 1531–1540, 2018, doi: 10.11591/ijece.v9i3.pp1531-1540.

[5] O. Chekira, A. Boharb, Y. Boujoudar, H. El Moussaoui, T. Lamhamdi, and H. El Markhi, "An improved energy management control strategy for a standalone solar photovoltaic/battery system," *Indo. J. of Elect. and Comp. Engg. (IJECE),* vol. 27, no. 2, pp. 647–658, 2022, doi: 10.11591/ijeecs.v27.i2.pp647-658.

[6] A. Mahmood Hadi, E. M. Thajeel, and Ali K. Nahar, "A novel optimizing PI control of shunt active power filter for power quality enhancement," *Bullet. of Elect. Engg. and Info.*, vol. 11, no. 3, pp. 1194–1202, 2022, doi: 10.11591/eei.v11i3.322.

[7] B. J. Abdulelah, Y. I. M. Al-Mashhadany, S. Algburi, and G. Ulutagay, "Modeling and analysis: power injection model approach for high performance of electrical distribution networks," *Bullet. of Elect. Engg. and Info.*, vol. 10, no. 6, pp. 2943–2952, 2021, doi: 10.11591/eei. v10i6.3126.

[8] A. Hinda, and M. Khiat, "Real-time simulation of static synchronous condenser (STATCOM) for compensation of reactive power," *Int. J. of Elect. and Comp. Engg. (IJECE),* vol. 10, no. 6, pp. 5599–5608, 2020, doi: 10.11591/ijece.v10i6.pp5599-5608.

[9] N. Patel, N. Gupta, A. Kumar, and A. Kumar Verma, "Multifunctional grid interactive solar photovoltaic systems: A comprehensive review," *Int. J. of Ren. Energy Research* (IJRER), vol. 8, no. 4, pp. 2116-30, 2018, doi: 10.20508/ijrer.v8i4.8404.g7517.

[10] N. Patel, N. Gupta, and R.C. Bansal, "Combined active power sharing and grid current distortion enhancement-based approach for grid-connected multifunctional photovoltaic inverter," *Int. Trans. on Elect. Energy Sys.*, vol. 30. no. 3, 2020, doi: 10.1002/2050-7038.12236.

[11] H. D. Tafti, A. I. Maswood, G. Konstantinou, J. Pou and F. Blaabjerg, "A general constant power generation algorithm for photovoltaic systems," *IEEE Trans. on Power Elect*., vol. 33, no. 5, pp. 4088–4101, 2018, doi: 10.1109/TPEL.2017.2724544.

[12] I. Hussain, M. Kandpal, and B. Singh, "Real-time implementation of three-phase single-stage PV grid-tied system using TL-VSC", *IET Rene. Power Gen.*, vol. 11, pp. 1576–1583, 2017, doi: 10.1049/iet-rpg.2016.0871.

[13] R. K. Agarwal, I. Hussain, and B. Singh, "Dual-function PV-ECS integrated to 3P4W distribution grid using 3M-PLL control for active power transfer and power quality improvement," *IET Rene. Power Gen.*, vol.12, no. 8, pp. 920–927, 2018, doi: 10.1049/iet-rpg.2016.0723.

[14] G. Bhuvaneswari, and Manjula G. Nair, "Design, simulation, and analog circuit implementation of a three-phase shunt active filter using i-cosφ algorithm," *IEEE Trans. Power Delivery*, vol. 23, no. 2, pp. 1222–1235, 2008, doi: 10.1109 /TPWRD. 2007.908789.

[15] M. Karimi-Ghartemani and H. Karimi, "Processing of symmetrical components in time-domain," in *IEEE Trans. on Power Systems*, vol. 22, no. 2, pp. 572–579, 2007, doi: 10.1109/TPWRS.2007.894860.

[16] H. Akagi, Y. Kanazawa, and A. Nabae, "Instantaneous reactive power compensators comprising switching devices without energy storage components," *IEEE Trans. Ind. Appl*., vol. 20, no. 3, pp. 625–630, 1984, doi: 10.1109/TIA.1984.4504460.

[17] N. E. Zakzouk, A. K. Abdelsalam, A. A. Helal and B. W. Williams, "PV single-phase grid-connected converter: DC-link voltage sensorless prospective", *IEEE J. of Emer. and Sele. Topics in Power Elect.*, vol. 5, no. 1, pp. 526–546, 2017, doi: 10.1109/JESTPE.2016.2637000.

[18] A. Alizadeh Asl, and R. Alizadeh Asl, "Modeling and control of a hybrid DC/DC/AC converter to transfer power under different power management strategies", *Int. J. of Power Elect. and Drive System (IJPEDS),* vol. 12, no. 3, pp. 1620–1631, 2021, doi: 10.11591/ijpeds.v12.i3.pp1620-1631.

[19] M.R. Bengourina, M. Rahli, S. Slami, L. Hassaine, "PSO based direct power control for a multifunctional grid connected photovoltaic system," *Int. J. of Power Elect. and Drive System (IJPEDS)*, vol. 9, no. 2, pp. 610–621, 2018, doi: 10.11591/ ijpeds.v9.i2.pp610-621.
[20] I. Yadav, S. Kumar Maurya, and G. K. Gupta, "A Literature review on industrially accepted MPPT techniques for solar PV system," *Int. J. of Elect. and Comp. Engg (IJECE)*, vol. 10, no. 2, pp. 2117–2127, 2020, doi: 10.11591/ijece.v10i2.pp2117-2127.
[21] M. Moutchou and A. Jbari, "Fast photovoltaic Inc Cond-MPPT and backstepping control, using DC-DC boost converter," *Int. J. of Elect. and Comp. Engg (IJECE)*, vol. 10, no. 1, pp. 1101–1112, 2020, doi: 10.11591/ijece.v10i1.pp1101-1112.
[22] F. El Otmani *et al*., "Sensorless integral sliding mode control of single-phase grid-connected PV system," *IFAC-Papers*, vol. 54, no. 21, pp. 49–54, 2021, doi: 10.1016/j.ifacol.2021.12.009.
[23] J. Yuan, F. Gao, and H. Gao, "DC voltage sensorless control strategy of grid-tied two-stage three-phase photovoltaic system," *8th IEEE Int. Conf. on Power Elect.-ECCE Asia*, pp. 1908–1912, 2011, doi: 10.1109/ICPE.2011.5944408.
[24] V. Kumar, and M. Singh, "Sensorless DC-link control approach for three-phase grid integrated PV system," *Int. J. of Elect. Power & Energy Systems*, vol. 112, pp. 309–318, 2019, doi: 10.1016/j.ijepes.2019.05.006.
[25] C. Jain, and B. Singh, "A three-phase grid tied PV system with adaptive DC link voltage for CPI voltage variations," *IEEE Trans. on Sus. Energy*, vol. 7, no.1, pp. 337–344, 2015, doi: 10.1109/TSTE.2015.2496297.
[26] A. Chaithanakulwat, "Development of DC voltage control from wind turbines using proportions and integrals for three-phase grid-connected inverters," *International Journal of Electrical and Computer Engineering*, vol. 10, no. 2, pp. 1701–1711, 2020, doi: 10.11591/ijece.v10i2.pp1701-1711.

BIOGRAPHIES OF AUTHORS

Meghraj Morey is working as a Assistant Professor in Government College of Engineering Aurangabad, (M.S.) India since 2010. He received the bachelor's degree in Electrical Engineering from Amravati University in 2001, the master's degree in Electrical Engineering from Mumbai University in 2006, and he is currently working toward the Ph.D. degree from Malviya National Institute of Technology, Jaipur, India. His research areas include grid integrated PV system, power quality issues, active power filter, harmonics mitigation techniques, power electronics, electric drives. He can be contacted at email: 2021ree9065@mnit.ac.in.

Nitin Gupta received Ph.D. (Electrical Engineering) from Indian Institute of Technology (IIT) Roorkee. He is currently working as an Assistant Professor at the Department of Electrical Engineering, Malviya National Institute of Technology, Jaipur, India. His research areas include Power Electronics and Drives, Power Quality, Electrical Machines, Active Power Filter, Harmonic Mitigation Techniques, AI Techniques Applications to Power Electronics, Power conversion techniques for renewable energy system, Multi-Level Inverters. He has been serving as a reviewer for many highly-respected journals. He can be contacted at email: nitingupta.ee@mnit.ac.in.

Man Mohan Garg received his B.E. (Electrical Engineering) from the M.B.M. Engineering College Jodhpur, India, in 2008. He received his M.Tech. in Electrical Drive and Power Electronics from the Indian Institute of Technology (IIT) Roorkee, India, in 2010. He has completed his Ph. D. from Electrical Engineering Department of IIT Roorkee, India. His current research interests include design, modeling and control of DC–DC power converters, photovoltaic integration, and dc microgrid. He can be contacted at email: mmgarg.ee@mnit.ac.in.

Ajay Kumar (Member, IEEE) received the B.Tech. degree in Electrical and Electronics Engineering from Kurukshetra University, Kurukshetra, India, in 2012, and M.Tech. degree in power systems and the Ph.D. degree in electrical engineering from the Malaviya National Institute of Technology Jaipur, Jaipur, India, in 2016 and 2020, respectively. Since August 2021, he has been an Assistant Professor with the Department of Electrical and Electronics Engineering, Birla Institute of Technology Mesra, Ranchi, India. His research interests include distributed generation, integration of renewable energy sources, and power quality assessment and improvement. He can be contacted at email: ajaykumar.ee@bitmesra.ac.in.